Molecular dynamics simulations of complex-shaped particles using Voronoi-based spheropolyhedra

S. A. Galindo-Torres* and D. M. Pedroso†
School of Civil Engineering, The University of Queensland, Brisbane, Queensland 4072, Australia
(Received 22 February 2010; published 10 June 2010)

The spheropolyhedra method has been used earlier for efficient and accurate molecular dynamics simulations of granular matter with particles with complex shapes. Also the Voronoi construction is a tool of proved utility for the virtual representation of powders and grains. In this paper a technique that combines the two methods and provides a framework for the study of the three-dimensional mechanical behavior of granular matter is proposed. In order to understand the capabilities of the new method, a number of computer simulations of the cubic (true) triaxial test, measuring the mechanical behavior of packing of particles, is carried out. Results from tests with packing of complex-shaped particles represented by "Voronoi particles" are compared with corresponding results of packing of spherical particles. Features such as the saturation value for the macroscopically observed coefficient of friction, as reported in the literature, are compared for the packing of spheres and for the packing of "Voronoi particles," showing that the difference in shape strongly affects the results. The proposed technique and simulation results can be used to help understand how the individual shape of grains affects the macroscopic mechanical behavior of granular matter such as cohesionless soils.

DOI: 10.1103/PhysRevE.81.061303 PACS number(s): 45.70.−n, 47.11.Mn, 02.70.Ns, 45.40.−f

I. INTRODUCTION

The accurate representation and understanding of the mechanical behavior of granular matter, such as cohesionless soils, has been subject of intense research by physicists and engineers. There are two main branches of research on this topic: (a) based on the continuum mechanics which regards the matter as a solid body that deforms under external actions and has a continuum distribution of stress and strain; and (b) based on the discrete mechanics which regards matter as a set of independent particles as represented by the molecular dynamics approach. The first one is probably more common among engineers, mainly due to a practical limitation regarding computer power. Nonetheless, the second one, based on discrete mechanics, is gaining increasing attention among scientists mainly because the need of better understanding of the micromechanical aspects, but also due to the increasing power of new hardware.

In particular, the molecular dynamics method developed by Loup Verlet more than 50 years ago [1] was proposed to be used for the study of granular matter by Cundall [2] in the appendix of his Ph.D. thesis from the 1971. The advantages of methods based on this approach are many. For example, the stress network inside the medium can be observed, represented, and virtually measured [3]. In addition, heterogeneous materials can be considered easily by changing the elastic properties of each individual particles.

In the discrete approach, the interactions between grains are modeled by means of their individual properties (Young modulus, restitution coefficient, etc). Moreover, Newton's law is taken in account through the introduction of elastic, viscous, and frictional forces. These purely microscopical interactions, at the end, control the macroscopic behavior of the material. However, the direct relation between the microscopic and macroscopic features is not well understood yet. With this goal in mind physicists and engineers created the *Association pour L'Etude de la Micromecanique des Milieux Granulaires* which is responsible for the organization of the conference *Powders and Grains* each four years. The main goal is to improve understanding on this issue.

Basically, most of the simulations around are based on two-dimensional (2D) models with circular particles due to the fact that the simulations, in this limited condition, are less computational expensive than the three-dimensional ones [4–6]. Moreover, the representation of circular particles is way simpler than particles of complex shapes.

Nonetheless in two dimensions, the representation of more complex particles is possible by using Voronoi constructions [7–11]. In this approach, the Voronoi polygons requires an elastic force that is proportional to the overlapping area of the polygons, and hence cannot be derived from a potential function [12]. Note that disks do not have that problem since the elastic force is proportional to an overlapping length; however the generality of shapes is lost.

In three dimensions, particles with spherical shapes are the most commonly used. However their geometry is obviously restricted, and low void ratios would require large number of particles and also size distribution with a high dispersion (polydisperse). Some recent studies, however, have introduced a rolling resistance for spheres [13,14] in order to simulate the effect of general shaped grains in a simplistic way.

Regarding the mechanical behavior of packing of particles, either of spherical or complex shapes, one important investigation is the measurement of the stresses and strains generated by the so-called true triaxial test [15–18]. When using spherical particles, one must observe the strong limitation due to the rolling resistance method usually adopted which, although effective, is not clear and lacks physical significance.

In this paper the authors present an extension of the spheropolyhedra approach developed by Pourning [19], Alonso-Marroquin [20] and Galindo-Torres [21] and com-

*s.galinotorres@uq.edu.au
†d.pedroso@uq.edu.au

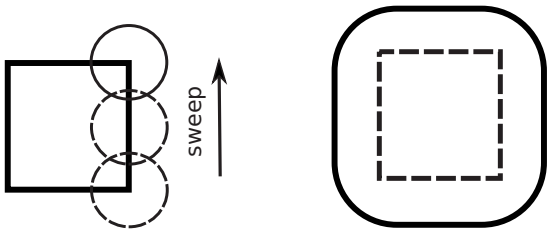

FIG. 1. Dilation of a square by a disk. The disk sweeps the profile of the square producing a larger square with rounded corners.

bine this method with the Voronoi construction. This technique allows for the study of the mechanical behavior of packing of complex particles, in addition to packing of spheres, as measured in true triaxial tests. Here it is shown how this method can represent complex geometries relatively easily.

In Secs. II–IV it is explained how to build a molecular dynamics algorithm based on the discrete element method (DEM), which regards particles of general shapes by employing the spheropolyhedra technique proposed here. Details of the two methods, spheropolyhedra and Voronoi construction, that are the central features of this paper, are introduced in these sections. Sections V and VI show the true triaxial test (TTT) simulations and some initial results on mechanical behavior of cohesionless soils. In Sec. VII, we present a study on the effect of shape on the macroscopic friction obtained from TTT simulations. Finally, Sec. VIII provides some conclusive discussions and possible projections of this work.

II. SPHEROPOLYHEDRA

To introduce the spheropolyhedra, some elements from mathematical morphology [22] are needed. Mathematical morphology has been used extensively in image processing algorithms as a way to qualitatively describe geological data [23]. It also provides the tools for simple operation like expansion and shrinking of image features. Here it is presented how this can be used to generate complex-shaped particles for molecular dynamics simulations as when employing the discrete element method.

A. Dilation

The "dilation" operation is first described. Given a polygon A in 2D [or three-dimensional (3D)] spaces and a disk B,

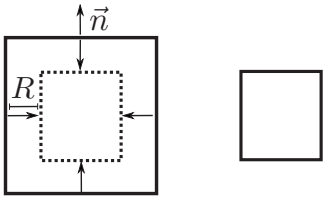

FIG. 2. Erosion of a square by a disk. In the erosion the square is shrunk by moving its sides inward (the opposite direction of the normal vector $\vec{n}$) by a distance R. This distance R corresponds here to the radius of the spheropolyhedra desired.

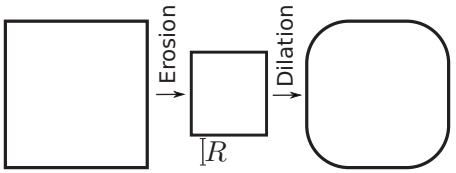

FIG. 3. Opening of a square by a disk. First the left square is eroded resulting in a smaller square. Then this smaller square is dilated. Both operators are carried out using the same spheroradius R.

the dilation of A by B (denoted as $A \oplus B$) is the new set obtained from sweeping the disk around the profile of the polygon. The result of this operation is a larger square with rounded corners, as illustrated in Fig. 1 for a particular situation.

B. Erosion

Second, the erosion is also a binary operation between two sets, in which the effect of eroding (denoted by $A \ominus B$) is equivalent to shrinking a geometric feature by moving all of its sides inward, and parallel to the normal vector at each side; here this distance is set to be equal to the radius of a circle representing feature B. For instance, Fig. 2 presents a particular case where a polygon is eroded by a disk and the final result is a smaller square.

C. Opening

Third, the opening of a geometric feature A by another B is just a combination of the previous two operations: first A is eroded by B and then the result is dilated. In mathematical notation,

$$A \circ B = (A \ominus B) \oplus B. \tag{1}$$

For example, In Fig. 3 it is observed that the "opening" of a square by the disk results in a square of similar dimensions but with rounded corners. All these mathematical morphology operations can be obviously extended to three dimensions in order to create a "spheropolyhedra"—the dilation or opening of polyhedra by a sphere. For instance, Fig. 4 shows a cube being initially eroded and then swept by a sphere in order to generate a "spherocube." Some additional examples of spheropolyhedra that can be readily obtained with this technique are given in Fig. 5.

III. VORONOI CONSTRUCTION

The Voronoi tessellation [24] has been used for many applications; from computer graphics [25] to geographical in-

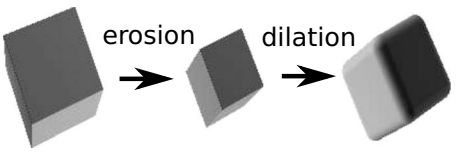

FIG. 4. The opening of a 3D particle: initially the cube is eroded, and then is dilated by a sphere.

FIG. 5. Some examples of spheropolyhedra. Left: sphero-"*rice*" (edge ⊕ sphere). Center: spherotetrahedron (tetrahedron ⊕ sphere). Right: sphero-"*star*" (three perpendicular edges ⊕ sphere).

formation systems (GIS) [26]. For the construction of particles, its application goes from the study of fragmentation processes [8], the study of the incremental response of soils [9], and the simulation of the hydraulic fracturing process [11].

The Voronoi construction method ensures that the packing will be totally closed and but with a random configuration. Its fundamentals are simple: a set of points, called Voronoi points, are randomly distributed over the space; then the polyhedron corresponding to a given Voronoi point is the set of points in the space that are closer to this particular Voronoi point than to any other [24]. This is done by drawing a line at the middle point of the segments that join two neighbor points and perpendicular to them, until a convex and close polygon is obtained. Figure 6 shows a packing (in 2D) generated with this method.

To obtain Voronoi spheropolyhedra, the Voronoi polyhedra must be dilated by a sphere element as shown in Sec. II. However, since the Voronoi packing is a closed one, the polyhedra generated are already all in contact with each other. Dilating the polyhedra will generate a undesirable initial overlap. In order to avoid this, each polyhedron must be initially eroded and then dilated, or equivalently, opened as explained in Sec. II. In Fig. 7, a particular Voronoi packing obtained using this method is shown.

The same operation can be applied when dealing with three dimensions. A particular example is presented in Fig. 8 in which the opening of an initial closed Voronoi packing is applied.

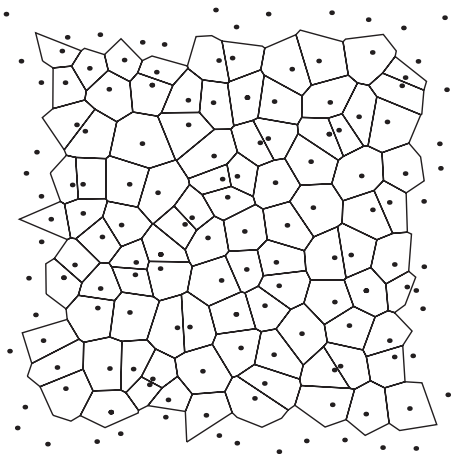

FIG. 6. The Voronoi construction explained. The points are randomly distributed in a plane and then their corresponding Voronoi polygons are built by bisecting the joining lines between the given points and its closer neighbors until a convex and closed polygon is obtained.

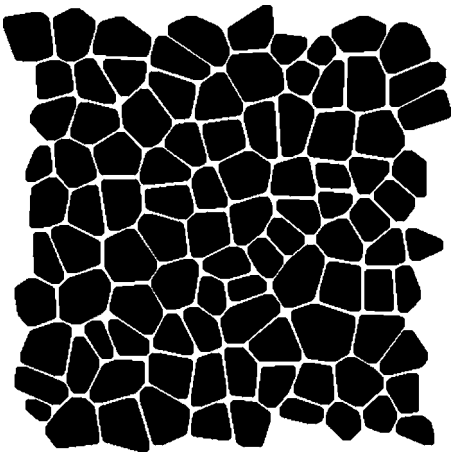

FIG. 7. The opened Voronoi grid. For visual aid the radius of the dilating disk is smaller than the eroding one. In this study the two radii are equal an there are not void spaces between the grains except for the rounded corners.

When necessary, to obtain a relative uniform distribution of volumes, the space can be divided in an cubic grid of cells with size l_u and a single Voronoi point dwells in each one of these cells. A typical cumulative distribution for the grains volumes obtained with this method is presented in Fig. 9.

IV. CONTACT LAW

The best advantage of the spheropolyhedra technique is that it allows for an easy and efficient definition of contact laws between the particles. This is due to the smoothing of the edges of all geometric features by circles or spheres.

Regarding the contact between two generic particles P_1 and P_2, first one has to consider the contact between each

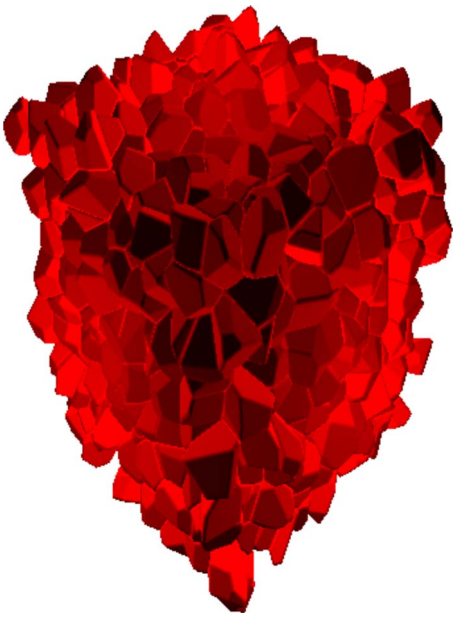

FIG. 8. (Color online) A three-dimensional array of Voronoi spheropolyhedra.

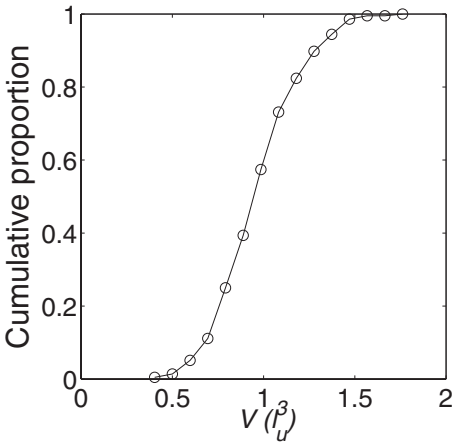

FIG. 9. Cumulative distribution of volumes for the Voronoi ensemble. The volume is given in length units, where one length unit is the cell side of the original cubic grid used for the generation.

geometric feature of particle P_1 with all features of particle P_2. In mathematical notation, both P_1 and P_2 have a set of vertices $\{V^i_{1,2}\}$, edges $\{E^j_{1,2}\}$, and faces $\{F^k_{1,2}\}$. Thus, a particle is defined as a polyhedron, i.e., a set of vertices, edges and faces, where each one of these geometrical feature is dilated by a sphere.

For simplicity, lets denominate the set of all the geometric features of a particle as $\{G^i_{1,2}\}$. Now the function representing this topology can be defined as the distance function for two geometric features according to

$$\mathrm{dist}(G^i_1, G^j_2) = \min[\mathrm{dist}(\vec{X}_i, \vec{X}_j)], \tag{2}$$

where $\vec{X}_i$ is a 3D vector that belongs to the set G^i_1. This means that the distance for two geometric features is the minimum Euclidean distance assigned to two points belonging to them.

Since both particles are dilated by their spheroradii R_1 and R_2, it can be said that there is a complete contact when the distance between the two geometric features is less than the addition of the corresponding radii used in the sweeping stage, i.e.,

$$\mathrm{dist}(G^i_1, G^j_2) < R_1 + R_2. \tag{3}$$

Here, the advantage of the spheropolyhedra technique becomes evident since this definition is similar to the one for the contact law of two spheres [15].

Now, suppose that the minimum distance for the sets G_1 and G_2 is given by the Euclidean distance between two of their points $\vec{X}_1$ and $\vec{X}_2$. This allows for the definition of a normal vector $\vec{n}$ given by

$$\vec{n}(G^i_1, G^j_2) = \frac{\vec{X}_2 - \vec{X}_1}{\|\vec{X}_2 - \vec{X}_1\|}. \tag{4}$$

With this definition, the same expression for the forces defined in conventional DEM codes (for spheres only), can be easily employed in this method. For example, we can assume a normal elastic force $\vec{F}_n$ proportional to the overlapping length (see e.g., [15]) defined according to

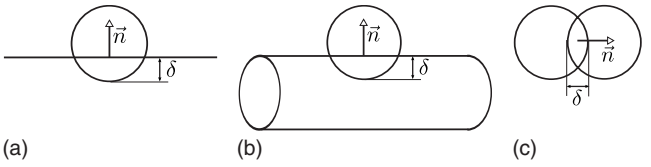

FIG. 10. The three different overlapping distances δ and their possible normal vectors $\vec{n}$ (a) In the case of the interaction of a spherovertex with a spheroplane the overlapping distance is always the penetration of the first into the second. (b) The collision of two spheroedges is taken as the collision of two cylinders. (c) The special case of two spheres considered as the collision of two spherovertices.

$$\vec{F}_n(G^i_1, G^j_2) = K_n \delta(G^i_1, G^j_2) \vec{n}(G^i_1, G^j_2), \tag{5}$$

in which K_n is a parameter called the normal stiffness and

$$\delta = \mathrm{dist}(G^i_1, G^j_2) - R_1 - R_2 \tag{6}$$

is the overlapping distance between the two geometric features.

The previous normal force is defined for a pair of geometric features. The net elastic force is the addition of all these forces for each possible pair of geometric features. However, for general polyhedra, it is only necessary to consider the interactions between vertices and faces and the interaction between edges and edges. The net elastic force is expressed as

$$\vec{F}_n(P_1, P_2) = \sum_{F^i_1, V^j_2} \vec{F}_n(F^i_1, V^j_2) + \sum_{V^i_1, F^j_2} \vec{F}_n(V^i_1, F^j_2) + \sum_{E^i_1, E^j_2} \vec{F}_n(E^i_1, E^j_2),$$

where only the necessary interactions are included in the summation. Figures 10(a) and 10(b) illustrate these two types of interactions.

In the spheropolyhedra formalism, a sphere is just a set containing one vertex positioned at the center of the sphere. The spheroradius is equal to the radius of the sphere and the interaction considers only the vertex-vertex interaction,

$$\vec{F}_n(P_1, P_2) = \vec{F}_n(V_1, V_2),$$

as explained in Fig. 10(c).

Likewise, frictional forces are simply introduced by means of the Cundall-Strack spring method [27], where there is a static friction force given by an incremental tangential displacement $\vec{\varepsilon}$, defined according to

$$\vec{F}_t = K_t \vec{\varepsilon} \tag{7}$$

in which K_t is the tangential stiffness and $\vec{\varepsilon}$ has a incremental change defined as follows:

$$d\vec{\varepsilon} = \vec{v}_t dt, \tag{8}$$

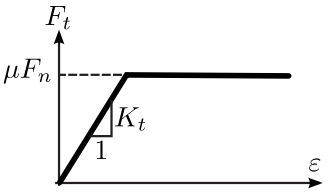

FIG. 11. The value of the tangential force F_t grows proportionally to the displacement ε but when the Coulomb threshold (μF_n) is reached, it immediately takes this value.

Here, dt is the time step and $\vec{v_t}$ is the component of the relative velocity at the point of contact that is tangential to the normal vector given by Eq. (4). When $\|\vec{F_t}\| > \mu\|\vec{F_n}\|$, then the force takes the Coulomb value and hence the dynamical friction is introduced as illustrated in Fig. 11

Another (viscous) force is introduced here to account for the proper stability of the simulation. This is defined according to

$$\vec{F_v} = g_n\vec{v_n} + g_t\vec{v_t} \tag{9}$$

in which, g_n and g_t are the normal and tangential viscous coefficients, respectively, and $\vec{v_n}$ is the normal component of the relative velocity at the point of contact.

Finally, all these forces are added to obtain the net force over a particle. Afterward, Newton's second law is solved for which here the Verlet algorithm is employed [1]. Each of these forces also provide the torque, where the point of application is at the middle of the line connecting the two contact points for each pair of geometric features that are in contact. With the torque, the angular dynamical equation of movement is solved with the Leap Frog algorithm [21].

V. CUBIC (TRUE) TRIAXIAL TEST

The spheropolyhedra approach allows for an easy way to model polyhedral shapes. In particular, planes can be modeled as a set of four vertices, four edges and one face. The method permits to consider the plane as just another particle subjected to the same contact law and dynamical equations. Hence, an elemental test like the true triaxial test (TTT) can be easily simulated, since it can be represented by a box with six walls (lids) and each lid can be simply modeled as a particle; i.e., nothing has to be changed to add these walls to a simulation.

In the true triaxial test, an ensemble of Voronoi grains are put inside a box made from six planes. Figure 12 shows the experimental setup and how to measure some important quantities from this test.

Some important quantities commonly used to analyze the results of true triaxial tests [18] are defined as follows: the mean (p) and deviatoric (q) stress invariants and the volumetric (ε_v) and deviatoric (ε_d) strains according to

$$p = \frac{\sigma_1 + \sigma_2 + \sigma_3}{3}, \tag{10}$$

$$q = \sqrt{\frac{(\sigma_1 - \sigma_2)^2 + (\sigma_1 - \sigma_3)^2 + (\sigma_2 - \sigma_3)^2}{2}}, \tag{11}$$

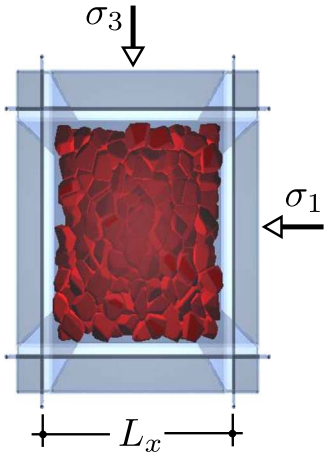

FIG. 12. (Color online) The test setup, the Voronoi array is put inside the rectangular box composed by six planes. The stresses, lateral σ_1, frontal σ_2 (not shown but applied to the front and back planes) and vertical σ_3, are applied to the planes and a triaxial test can be simulated. To measure the strain in the x direction, ε_1, the change in the initial length ΔL_x is divided by the initial length L_x.

$$\varepsilon_v = \varepsilon_1 + \varepsilon_2 + \varepsilon_3, \tag{12}$$

$$\varepsilon_d = \sqrt{\frac{2}{3}[(\varepsilon_1 - \varepsilon_2)^2 + (\varepsilon_1 - \varepsilon_3)^2 + (\varepsilon_2 - \varepsilon_3)^2]}, \tag{13}$$

in which σ_i are the principal stress invariants and ε_i the principal strain invariants. Here, extension is taken as positive.

In the true triaxial test, the sample is initially subjected to a constant isotropic compression p with zero deviatoric stress (q=0). Afterward, shearing is developed by applying different combinations of (principal) stresses.

The isotropic compression phase is illustrated in Fig. 13 by a p versus q plot: stress path [Eq. (1)]. This is achieved by keeping the three stresses constant at the same value and moving all lids (walls) at the same speed.

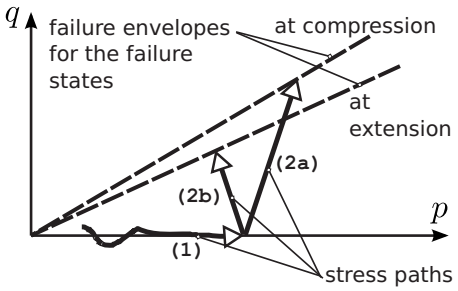

FIG. 13. In a q vs p plane the TTT has two stages for both the compression and extension tests: (1) an isotropic compression is applied by setting σ_1=σ_2=σ_3; (2a) by applying a constant strain rate in the z direction compressing the volume, σ_3 increases and therefore p and q values also increase proportionally until the failure is reached; and (2b) The strain rate in the z direction now extends the volume and q increases while p decreases. The dashed lines are the failure envelopes, and join the origin with the failure points.

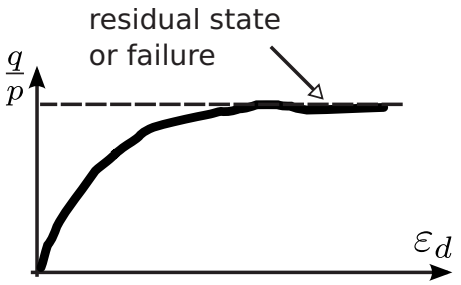

FIG. 14. Typical response of the stress ratio in a true triaxial test.

The shearing phase is accomplished by applying a constant strain rate ($\dot{\varepsilon}_3$=constant) along the z axis. This is done by moving the pair of planes perpendicular to the z direction with constant velocity. Two stress paths developed during shearing are presented in Fig. 13, (2a) and (2b). The first one corresponds to compression and the other to extension. The compression happens by keeping two stress components constant and increasing the other one by compressing the sample at a constant strain rate in one direction. On the other hand, the extension is achieved by the same way but with a controlled strain that ensures expansion of the sample.

In Fig. 14 the typical behavior expected for a pack of loose cohesionless soils, depicted by the relationship between the stress rate (q/p) versus the deviatoric strain is presented. Initially there is an elastic region where the stiffness (proportional to the slope of this curve) has its highest value, but then the failure occurs and the soil enters the plastic regime where the stress ratio takes a constant value. Traditionally, these final constant value state is called "residual" state [28].

VI. ELEMENTARY TEST RESULTS

A first true triaxial test simulation is carried out with a sample made from an array of 216 Voronoi spheropolyhedra. The simulation parameters are shown in Table I. The results for this simulation are presented in Fig. 15(a) where the stress ratio q/p vs the deviatoric strain ε_d is shown. The behavior resembles a dense soil response since the stress ratio increases until it reaches a peak value and then it is relaxed to a residual value.

Figure 15(b) shows the volumetric strain ε_v evolution. The result is somehow expected for this configuration: the volume increases always showing pure dilatancy. This is due

TABLE I. Set of parameters used in the simulations.

Parameter	Value
K_n	1.e5 N/m
K_t	5.e4 N/m
l_u	1 cm
g_n	1.6 kg/s
g_t	0.0 kg/s
Density	3.0 g/cm^3

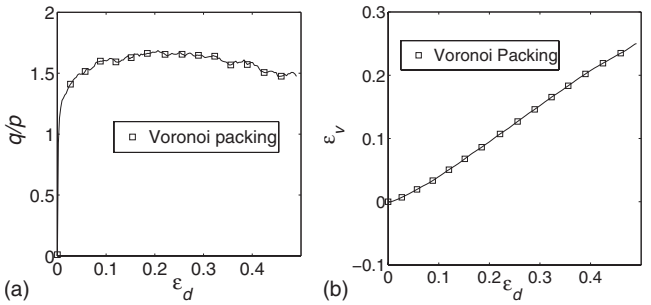

FIG. 15. The results with one particular triaxial test with a confining pressure of $1.0e^{-4}K_n$ on a compression path.

to the closed packing used here which already has the minimum possible volume; in this case the only freedom of movement lies on its expansion. Note that it is difficult to reproduce the pure compression behavior with the code presented here due to this "densest" state achieved by the Voronoi packing.

These initial results shows that the Voronoi packing behaves like a granular material under applied stress. Nonetheless, to further investigate the macroscopic friction angle, several tests with different initial confining pressures are considered, since the mechanical behavior of granular matter is highly dependent on confining. Moreover, to add a little statistical difference among samples, the Voronoi packing is generated with different seeds for the random number generator.

In total, eight different samples composed by Voronoi particles were simulated, each with different initial confining pressures p. Figure 16 presents all the stress paths applied in these tests, including compression and extension ones. The end points of each path are connected for each compression or extension set, resulting on "envelopes of failure" (dashed lines in Fig. 16). These envelopes, allow for the measurement of the so-called macroscopic friction angle through the following expression (Drucker Prager Criterion [29]),

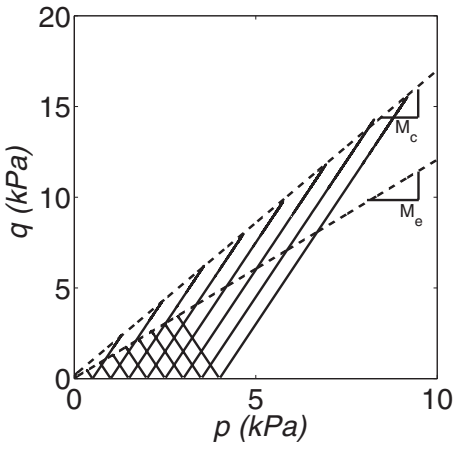

FIG. 16. Results from the true triaxial experiments for both compression (p increasing) and extension (p decreasing) showing the deviatoric stress q versus the isotropic stress (or pressure) p. The dashed lines join the failure points of each experiment and their slopes give the macroscopic friction angle. These lines however do not intersect at the origin giving a nonlinear effect.

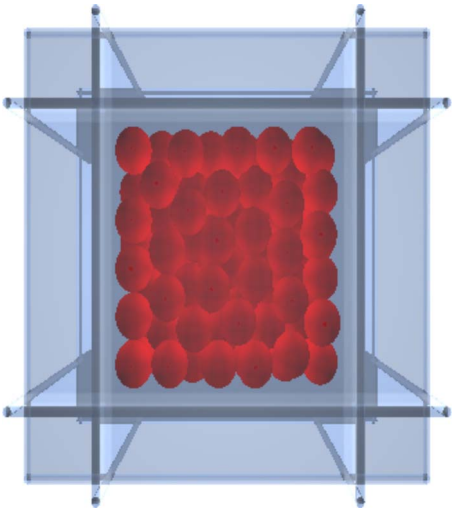

FIG. 17. (Color online) A similar test setup was made for spheres with the same number of particles, average mass and parameters.

$$\sin(\phi_{c,e}) = \frac{3M_{c,e}}{6 + M_{c,e}}, \tag{14}$$

in which $M_{c,e}$ is the slope of the (straight) failure envelopes and $\phi_{c,e}$ the macroscopic friction angle, that can be defined for either compression c or extension e.

The averaged macroscopic friction angle obtained is equal to $(41.06 \pm 2.01)°$ for the compression tests and $(30.06 \pm 1.85)°$ for the extension ones with a microscopic friction angle of 21.80°.

VII. EFFECT OF SHAPE ON MACROSCOPIC FRICTION

Following the thesis that shape generates a contribution to the macroscopic friction, thesis that has been evaluated before [21], simulations should be carried out with different geometries. Therefore a comparison is done between the results for the Voronoi packing with results obtained from an array of spheres (see Fig. 17), where the same number of particles, parameters and average mass were taken for this sample. They are subjected also to the same stresses, however they do not include the rolling resistance that is usually included in other studies [14] since our goal is to evaluate the effect of the shape on the macroscopic friction only and avoid "unphysical" behaviors.

The sample of spherical particles is prepared as follows: initially an hexagonal close packing is programmed and then some spheres are randomly removed until the desired number of particles is reached, giving a somehow loose packing.

Once both samples are prepared, some compression tests were applied for the Voronoi and the spherical arrays. The results are compared in Fig. 18 and, as expected, the spheres show less strength than the Voronoi packing. The spheres, without a rolling resistance, can roll over each other decreasing the effect of the microscopic friction a feature that is more difficult to achieve for the Voronoi packing since it is denser. Previous studies [30,31] have shown this behavior

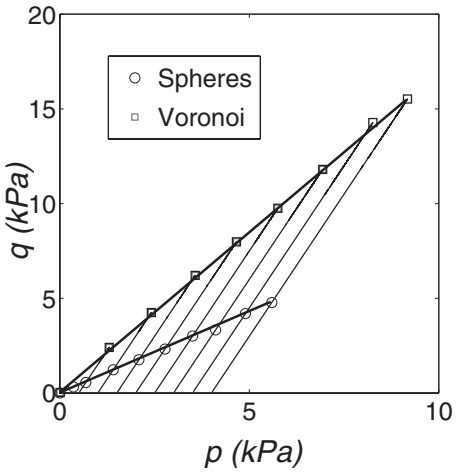

FIG. 18. Results for several compression tests on packing of spheres showing the failure points for both spheres (circles) and Voronoi spheropolyhedra (squares).

and have explained it by a high contribution of forces between polygonal edge-edge contacts in 2D and polyhedral face-face contacts in 3D that are not present in disks and spheres. Indeed in our case two Voronoi polyhedra in contact with a common side are less likely to roll over one another providing a greater strength for the soil.

It has been found in the literature that with spheres [32] the macroscopic friction coefficient μ_{macro} increases with the microscopic one μ_{micro} until a saturation value, where the rolling effect of spheres maintain μ_{macro} at a constant value independent of μ_{micro}. However, if there is a restriction to the rotation of the spheres like, for example, by completely stopping their rotation, this saturation point is not met [32]. To check this, we changed μ_{micro} between 0.0 and 0.8, for 8 different random samples per case in order to have good statistics. Also in these simulations the tangential viscous coefficient g_t of Eq. (9) is set to zero so the only dissipative force in the tangential direction is due to the Coulomb friction. In Fig. 19 the results of these simulations can be seen. As obtained in previous studies with spheres, the sphere soil reaches the saturation limit [32] of approximately 0.32 in this

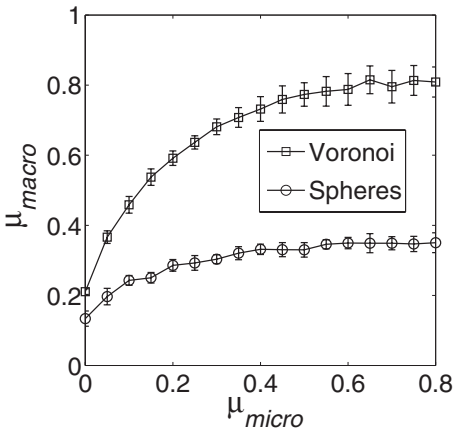

FIG. 19. Results for several true triaxial experiments in which the microscopic friction coefficient μ_{micro} is changed for both the Voronoi (squares) and the spheres (circles) arrays.

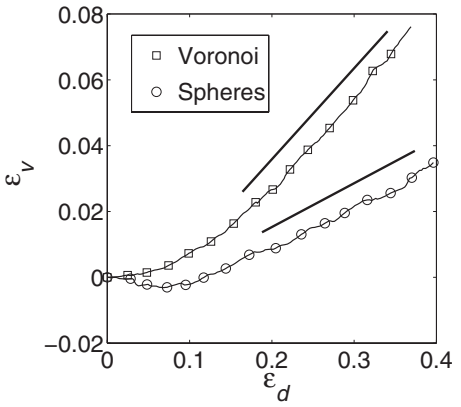

FIG. 20. Volumetric strain ε_v versus the deviatoric strain ε_d for both Voronoi grains (squares) and spheres (circles). Straight lines indicate the slope or dilatancy ψ at the plastic deformation regime. For the Voronoi packing the dilatancy value is $\psi=12.53°$ and for the sphere packing is $\psi=7.52°$.

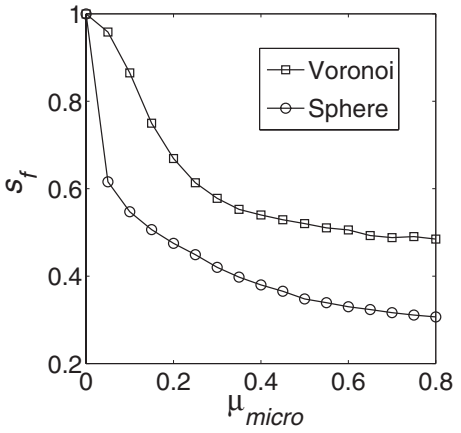

FIG. 21. Sliding contact fraction s_f versus the microscopical friction coefficient μ_{micro} for the Voronoi array (circles) and the sphere array (squares).

case. In the Voronoi case μ_{macro} goes higher and a saturation value is also observed at around 0.8. Another striking result is the existence of a residual μ_{macro} when μ_{micro} goes to zero. The absence of this residual friction has been assumed before [32], but in shear test simulations it has been found for disks in 2D [14] and spheres in 3D [33]. This residual friction comes from the initial packing and the interlocking of the different particles which is higher in the Voronoi array than in the sphere one. Regardless of the type of particle that is considered, even if the friction force is zero, there has to be some work done to move that particles in the compression (or extension) process.

To further check this hypothesis, the volumetric strain ε_v versus the deviatoric strain ε_d are shown for a simulation with $\mu_{micro}=0$ and $g_t=0$ in Fig. 20. As expected, the Voronoi array expands from the beginning while the sphere array, which is not as closely packed as the Voronoi one, initially is shrunk and only then it is expanded due to the shearing over the sample. The dilatancy ψ is defined as the slope of this curve in the plastic deformation regime and is shown in Fig. 20 by a set of straight lines. As can be seen the dilatancy for the Voronoi packing is higher than for the spherical one. This means that for the Voronoi packing a higher volume variation happens during shearing of the sample than with the spheres. This is due to the extra effort required to move the interlocked grains even if they can slide freely. The interlocking of the particles produce both, the residual μ_{macro} and the higher dilatancy in the Voronoi packing, as compared to the corresponding for the spheres packing.

The final analyses involve the *sliding contact fraction* s_f, defined as the ratio between the contacts that are in the Coulomb dynamic friction regime over the total number of sliding contacts. This total number of contacts is determined by identifying those contacts that have reached the Coulomb threshold (see Fig. 11). To observe the influence of the microscopic friction μ_{micro} on the sliding contact fraction s_f, simulations of packings of Voronoi and spheres particles are carried out. The results are presented in Fig. 21.

As expected, it is observed that when $\mu_{micro}=0$, the sliding fraction is equal to 1, meaning that all contacts are sliding. This is obvious if we remember that the Cundall-Strack friction [see Eq. (7)] was adopted here and that the threshold for the sliding contact is equal to zero always.

For spheres, s_f decreases rapidly with μ_{micro} and reaches its minimum value when the fraction of sliding contacts is less than 40%. This means that at this high friction threshold, the majority of spheres are rolling and not sliding and the saturation value observed in Fig. 19 is due to this rolling. The rolling of the spheres maintains μ_{macro} at a constant value.

It is found that the Voronoi packing behaves similarly as the spheres one. For higher values of μ_{micro} most of the contacts are not sliding. Moreover, μ_{macro} for the Voronoi packing also reaches a saturation point (see Fig. 19). The conclusion is that for the Voronoi packing the rolling of the grains also maintains μ_{macro} at a constant value independent of μ_{micro} if the latest is high enough. The only difference is in the saturation and residual values produced by the different geometry and packing, not in their general behavior.

VIII. CONCLUSIONS

The spheropolyhedra method combined with the Voronoi construction presented here is an efficient an easy to implement method that allows molecular dynamics simulations with particles of complex shapes. The true strength of the method comes from the versatility in the representation of smooth particles as a set of geometric features (vertices, edges and faces) rounded by spheres and that can interact with each other. This leads to a powerful multi contact approach and allows for the representation of nonconvex shapes. Due to the Voronoi construction, packings of closed structure (dense) can be generated with random configurations. Moreover, contrary to common practice, the code presented here does not require extra (unphysical) models for the so-called rolling resistance when dealing with spheres. This is due to the allowance for complex shapes as generated by the Voronoi packings.

The Voronoi packing offer other advantages. For example a void volume close to zero can be obtained since all the

grains are in complete contact with each other from the beginning. This is very difficult to achieve with packing of spheres only, for which a wide range of radii is required to ensure that the void spaces are filled with small spheres. This obviously increases the simulation time due to the increased number of particles required for the simulation.

The main conclusion of the present paper is that the representation of the correct geometry of the individual grains is important in molecular dynamics simulations since this affects the macroscopic response of the material. It is verified through a comprehensive set of simulations of the true triaxial test that the shape of the grains has impact on both the strength as well as the dilatancy properties of cohesionless soils. This is mainly due to the different structure achieved by the granular packings since the Voronoi construction ensures smaller void ratios than the monodisperse sphere array.

It is verified that the averaged macroscopic friction angle obtained in compression tests with Voronoi particles (complex shapes) is more or less equal to 1.9 times greater than the microscopic friction angle, introduced as a simulation parameter for the Coulomb law in the algorithm. For extension tests with complex shapes, the macroscopic friction angle is more or less 1.4 greater than the microscopic one. This proofs that the shape of the particles affects the structure of the packing and hence the strength of granular matter.

It is also verified that the macroscopic friction coefficient μ_{macro} reaches always a saturation point regardless of the microscopical one (μ_{micro}). For the spherical particles μ_{macro} is reached sooner than for the Voronoi packing but the behavior is similar. The cause of this saturation is the same, the rolling of the grains maintains the value of μ_{macro} constant for both spherical and Voronoi particles.

[1] L. Verlet, Phys. Rev. **159**, 98 (1967).
[2] P. A. Cundall, *A Computer Model for Simulating Progressive, Large-Scale Movements in Blocky Rock Systems*, in Proceedings of the Symposium of the International Society for Rock Mechanics (Nancy, France, 1971).
[3] R. García-Rojo, F. Alonso-Marroquín, and H. J. Herrmann, Phys. Rev. E **72**, 041302 (2005).
[4] P. A. Cundall and O. D. L. Strack, Geotechnique **29**, 47 (1979).
[5] H. Kruggel-Emden, E. Simsek, S. Rickelt, S. Wirtz, and V. Scherer, Powder Technol. **171**, 157 (2007).
[6] S. D. C. Walsh, A. Tordesillas, and J. F. Peters, Granular Matter **9**, 337 (2007).
[7] H. J. Tillemans and H. J. Herrmann, Physica A **217**, 261 (1995).
[8] F. Kun and H. J. Herrmann, Comput. Methods Appl. Mech. Eng. **138**, 3 (1996).
[9] F. Alonso-Marroquin and H. J. Herrmann, Phys. Rev. E **66**, 021301 (2002).
[10] J. A. Åström, B. L. Holian, and J. Timonen, Phys. Rev. Lett. **84**, 3061 (2000).
[11] S. A. Galindo-Torres and J. D. Muñoz Castaño, Phys. Rev. E **75**, 066109 (2007).
[12] T. Poeschel and T. Schwager, *Computational Granular Dynamics* (Springer, Berlin, 2004).
[13] M. Oda and K. Iwashita, Int. J. Eng. Sci. **38**, 1713 (2000).
[14] N. Estrada, A. Taboada, and F. Radjäi, Phys. Rev. E **78**, 021301 (2008).
[15] N. Belheine, J. P. Plassiard, F. V. Donzé, A. Darve, and F. Seridi, Comput. Geotech. **36**, 320 (2009).
[16] E. Q. Chowdhury and T. Nakai, Comput. Geotech. **23**, 131 (1998).
[17] T. Nakai and M. Hinokio, Soils Found. **44**, 12 (2004).
[18] D. M. Pedroso, Ph.D. thesis, University of Brasília, 2006.
[19] L. Pournin and T. M. Liebling, *Powders and Grains 2005* (Balkema, Leiden, 2005), pp. 1375–1478.
[20] F. Alonso-Marroquín, EPL **83**, 14001 (2008).
[21] S. A. Galindo-Torres, F. Alonso-Marroquín, Y. C. Wang, D. Pedroso, and J. D. Muñoz Castaño, Phys. Rev. E **79**, 060301(R) (2009).
[22] E. R. Dougherty, *Mathematical Morphology in Image Processing* (CRC, Boca Raton, FL, 1992).
[23] J. Serra, *Image Analysis and Mathematical Morphology* (Academic Press, Inc., Orlando, FL, 1983).
[24] L. J. Guibas, D. E. Knuth, and M. Sharir, Algorithmica **7**(1–6), 381 (1992).
[25] K. E. Hoff III, J. Keyser, M. Lin, D. Manocha, and T. Culver, in *Fast Computation of Generalized Voronoi Diagrams Using Graphics Hardware*, Proceedings of the 26th Annual Conference on Computer Graphics and Interactive Techniques (ACM, New York, 1999), p. 286.
[26] C. M. Gold, P. R. Remmele, and T. Roos, Lect. Notes Comput. Sci. **1340**, 21 (1997).
[27] P. A. Cundall and O. D. L. Strack, A discrete numerical model for granular assemblies, 1979.
[28] A. Schofield and P. Wroth, *Critical State Soil Mechanics* (McGraw Hill, New York, 1968).
[29] D. C. Drucker and W. Prager, Q. Appl. Math. **10**, 157 (1952).
[30] E. Azéma, F. Radjai, and G. Saussine, Mech. Mater. **41**, 729 (2009).
[31] E. Azéma, F. Radjaï, R. Peyroux, and G. Saussine, Phys. Rev. E **76**, 011301 (2007).
[32] A. S. J. Suiker and N. A. Fleck, ASME J. Appl. Mech. **71**, 350 (2004).
[33] P.-E. Peyneau and J.-N. Roux, Phys. Rev. E **78**, 011307 (2008).